

Geophysical Research Letters[®]

RESEARCH LETTER

10.1029/2022GL098547

Key Points:

- Energy conversion $\mathbf{j} \cdot \mathbf{E}'$ is around zero in quiet current sheet but nonzero in electron-only reconnection
- Ion temperature does not change in electron-only reconnection but peaks in standard reconnection
- We justify that the MMS 17 June 2017 event is a magnetotail electron-only reconnection event

Correspondence to:

S. Lu and Q. Lu,
lusan@ustc.edu.cn;
qmlu@ustc.edu.cn

Citation:

Lu, S., Lu, Q., Wang, R., Pritchett, P. L., Hubbert, M., Qi, Y., et al. (2022). Electron-only reconnection as a transition from quiet current sheet to standard reconnection in Earth's magnetotail: Particle-in-cell simulation and application to MMS data. *Geophysical Research Letters*, 49, e2022GL098547. <https://doi.org/10.1029/2022GL098547>

Received 4 MAR 2022
 Accepted 24 MAY 2022

Electron-Only Reconnection as a Transition From Quiet Current Sheet to Standard Reconnection in Earth's Magnetotail: Particle-In-Cell Simulation and Application to MMS Data

San Lu^{1,2} , Quanming Lu^{1,2} , Rongsheng Wang^{1,2} , Philip L. Pritchett³ , Mark Hubbert⁴, Yi Qi⁴ , Kai Huang^{1,2}, Xinmin Li^{1,2} , and C. T. Russell⁴ 

¹CAS Key Lab of Geospace Environment, School of Earth and Space Sciences, University of Science and Technology of China, Hefei, China, ²CAS Center for Excellence in Comparative Planetology, Hefei, China, ³Department of Physics and Astronomy, University of California, Los Angeles, CA, USA, ⁴Department of Earth, Planetary, and Space Sciences, University of California, Los Angeles, CA, USA

Abstract Standard magnetic reconnection couples with both electron- and ion dynamics. Recently, a new type of magnetic reconnection, electron-only reconnection without the coupling of ion dynamics, has been observed in space. Using a two-dimensional particle-in-cell simulation, we show that in the externally-driven magnetotail, electron-only reconnection is a transition from quiet current sheet to standard reconnection. We find that (a) energy conversion $\mathbf{j} \cdot \mathbf{E}'$ is around zero in quiet current sheet but nonzero in electron-only reconnection, and (b) ion temperature does not change across electron-only reconnection but peaks at the center of standard reconnection. These two differences can be used as criteria to distinguish magnetotail electron-only reconnection from quiet current sheet and standard reconnection, respectively. Based on the two criteria, we justify that the MMS 17 June 2017 event is a magnetotail electron-only reconnection event.

Plain Language Summary The Earth has a long stretched magnetic tail, that is, magnetotail, formed by the interaction between the geomagnetic field and the plasma (ions and electrons) wind originated from the Sun. At the center of the magnetotail, there is a current sheet flanked by two different topologies of magnetic field lines. Magnetic reconnection, a fundamental plasma process during which magnetic field line topologies change, can occur in this magnetotail current sheet. Based on computer simulations in the past 20 years, a standard reconnection model with both ion and electron dynamics has been established, which can well describe magnetic reconnection observed in the magnetotail. Recently, a new type of reconnection with solely electron dynamics has been observed to occur in the magnetotail. Here using computer simulations, we show that electron-only reconnection in the magnetotail is a transition from magnetotail current sheet to standard reconnection. Based on the simulation results, we give two criteria for identification of electron-only reconnection in spacecraft observations in the magnetotail, using which we justify that the MMS 17 June 2017 event is a magnetotail electron-only reconnection event.

1. Introduction

Magnetic reconnection is a process of rearrangement of magnetic field line topologies in plasmas during which magnetic energy is converted to particle kinetic energy (Birn & Priest, 2007; Yamada et al., 2010). A standard model has been proposed based on numerical simulations to describe magnetic reconnection in space, in which magnetic diffusion occurs both in a larger-scale ion diffusion region and a smaller-scale electron diffusion region (e.g., Birn et al., 2001; Hesse et al., 2001; Ma & Bhattacharjee, 2001; Pritchett, 2001; Shay et al., 2001). The standard model predicts that the ion diffusion region is usually characterized by bi-directional ion outflows and the Hall electric- and magnetic fields (e.g., Fu et al., 2006; Hoshino et al., 2001; Huang et al., 2010; Lu et al., 2010), which has been observed by in-situ spacecraft in Earth's magnetotail (e.g., Borg et al., 2005; Eastwood et al., 2010; Nagai et al., 2001; Øieroset et al., 2001). Simulations further show that the electron diffusion region, which is embedded at the center of the ion diffusion region, is characterized by fast electron outflow jets, electron crescent velocity distribution, nonzero magnetic-to-particle energy conversion $\mathbf{j} \cdot \mathbf{E}'$ (here $\mathbf{E}' = \mathbf{E} + \mathbf{V}_e \times \mathbf{B}$ is the nonideal electric field), etc. (e.g., Hesse et al., 2014; Shay et al., 2007; Zenitani

et al., 2011), and these characteristics have also been confirmed by spacecraft detections of the electron diffusion region in Earth's magnetotail (e.g., Torbert et al., 2018).

Standard reconnection has also been observed to occur in Earth's turbulent magnetosheath (e.g., Retinò et al., 2007; Stawarz et al., 2022). However, Phan et al. (2018) recently find that magnetic reconnection in the magnetosheath can exhibit only the electron dynamics, whereas the ion dynamics are absent. Such electron-scale magnetic reconnection without ion coupling is therefore referred to as electron-only reconnection (e.g., Pyakurel et al., 2019). Further studies have shown that electron-only reconnection occurs pervasively in turbulent plasmas, not only in the magnetosheath (Lu et al., 2021; Stawarz et al., 2019, 2022) but also at Earth's bow shock (Gingell et al., 2019, 2020).

Magnetic reconnection in the magnetotail, as mentioned above, has been observed to be in accord with the standard reconnection model with electron- and ion dynamics coupling. However, electron-only reconnection also exists in the magnetotail as detected by the Magnetospheric Multiscale (MMS) spacecraft on 17 June 2017 (Hubbert et al., 2021, 2022; Lu et al., 2020; Wang et al., 2020). By performing a two-dimensional (2-D) particle-in-cell (PIC) simulation, Lu et al. (2020) show that electron-only reconnection in the magnetotail is a transition phase from quiet current sheet to standard reconnection. Such a transition is the onset of magnetotail reconnection caused by the electron tearing mode instability (Pritchett, 2005a, 2005b, 2010; Birn & Hesse, 2014; Hesse & Schindler, 2001; Liu et al., 2014; Pritchett & Lu, 2018). However, Farrugia et al. (2021) argue that the MMS 17 June 2017 event is not an electron-only reconnection event but a standard reconnection event. Given the above controversy, here we study the transition from quiet current sheet to electron-only reconnection and then to standard reconnection using a 2-D PIC simulation, and then we use the simulation results to show that the MMS 17 June 2017 event is an electron-only reconnection event.

2. Simulation Model

We use a 2-D PIC simulation model. To put our simulation in a context of in-situ spacecraft observations, we use a current sheet coordinate system (L, M, N) . The simulation is performed in the L - N plane, and M is the out-of-plane direction. The size of the simulation domain is $-32d_i \leq L \leq 0$, $-8d_i \leq N \leq 8d_i$, where d_i is the ion inertial length evaluated using unit density n_0 . The initial configuration is the Lembège-Pellat current sheet (Lembege & Pellat, 1982) with magnetic potential $A_{0M}(L, N) = -B_0\delta \ln\{\cosh[F(L)(N/\delta)]/F(L)\}$ and density $n(L, N) = n_0 F^2(L) \operatorname{sech}^2[F(L)(N/\delta)] + n_b$, where $F(L) = \exp[\epsilon(L + 16d_i)/\delta]$, and $\epsilon = (B_N/B_0)_{N=0}$. We adopt the current sheet half-width $\delta = 2d_i$, the background density $n_b = 0.2n_0$, and $\epsilon = 0.04$. The ion-to-electron mass ratio is $m_i/m_e = 400$. Uniform initial electron and ion temperatures are adopted, with $T_{i0} = 0.4167m_iV_A^2$ and $T_{e0} = 0.0833m_iV_A^2$, where V_A is the Alfvén velocity evaluated using B_0 and n_0 . The grid size is $\Delta L = \Delta N = d_i/64$, the time step is $\Delta t = 0.00025\Omega_{i0}^{-1}$, and the speed of light is $c = 40V_A$.

An external driver is imposed by adding an out-of-plane electric field $E_M = \hat{E}_M(t)S(L)$ at the N boundaries. Here $\hat{E}_M(t)$ describes the time evolution of the driver, and $S(L)$ describes the spatial distribution of the driver. We adopt $\hat{E}_M(t) = 2a\omega B_0 \tanh(\omega t)/\cosh^2(\omega t)$ and $S(L) = \operatorname{sech}^2[(L + 16d_i)/D_L]$. The parameter a determines the size of the field line deformation region from the top and bottom N boundaries, the parameter ω dictates the timescale of the driver, and D_L is the half-width of the driver. We use $D_L = 5d_i$, $a = 2d_i$ and $\omega = 0.05\Omega_i$, where the ion cyclotron frequency $\Omega_i = eB_0/m_i$. Open boundary conditions are used at the L boundaries. The unit density n_0 is represented by 376 particles per cell, and about 1.5×10^9 particles per species are employed at the initial time.

3. Simulation Results

Figure 1a shows the initial configuration is the Lembège-Pellat current sheet with a nonzero normal magnetic field $B_N = 0.04B_0$ at the neutral plane $N = 0$. This normal magnetic field, although small, prevents magnetic reconnection from occurring because it stabilizes both the electron tearing mode (Galeev & Zelenyi, 1976) and the ion tearing mode (Lembege & Pellat, 1982; Pellat et al., 1991). Because of the external driver, the current sheet thins, and the current density increases, therefore, a thin current sheet is formed, for example, at $\Omega_i t = 63$ (Figure 1b). According to the magnetic field topology, magnetic reconnection has not started yet at this time. At $\Omega_i t = 68$, the magnetic field topology has changed, which indicates occurrence of magnetic reconnection (Figure 1c). However, this is the early phase of reconnection because the topological change is minor (the change in magnetic flux at

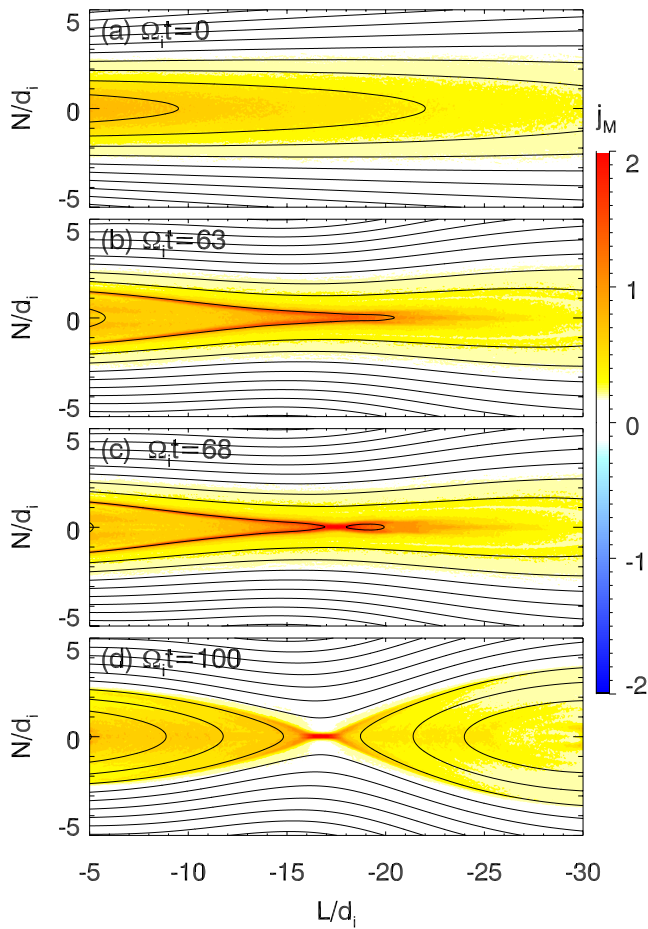


Figure 1. Out-of-plane current density j_M (in unit of en_0V_A) in the L - N plane in the (a) initial current sheet ($\Omega_i t = 0$), (b) quiet current sheet ($\Omega_i t = 63$), (c) preliminary reconnection ($\Omega_i t = 68$), and (d) well-developed reconnection ($\Omega_i t = 100$). The black curves represent the magnetic field lines in the L - N plane. In our simulation, the current density is in unit of en_0V_A .

the reconnection site from $\Omega_i t = 63$ to $\Omega_i t = 68$ is $\Delta\Psi = 0.034B_0d_i$). Reconnection then becomes dramatic, for example, at $\Omega_i t = 100$ (Figure 1d), with a significant topological change in the magnetic field (the change in magnetic flux at the reconnection site from $\Omega_i t = 63$ to $\Omega_i t = 100$ is $\Delta\Psi = 1.714B_0d_i$). Thus, magnetotail reconnection has three main phases – quiet current sheet, preliminary reconnection, and well-developed reconnection.

In the quiet current sheet at $\Omega_i t = 63$. Because of the external driver, the normal magnetic field B_N at the center of the current sheet decreases to around zero but is still positive, about $0.001B_0$ (Figure 2a, black curve), which allows occurrence of reconnection through the electron tearing mode instability. The thickness of the quiet current sheet is sub ion scale (Figure 3i, black curve). Therefore, a large fraction of the ions become demagnetized, whereas the electrons are mostly magnetized, forming a charge separation and thus an in-plane Hall electric field E_L and E_N (Figures 2 and 3b, black curves). The Hall electric field leads to an $\mathbf{E} \times \mathbf{B}$ drift in the $-M$ direction. Because the electrons are mostly magnetized, they follow the $\mathbf{E} \times \mathbf{B}$ drift (Figures 2 and 3h, black curves), and the ions are demagnetized and do not follow the $\mathbf{E} \times \mathbf{B}$ drift but follow the slower diamagnetic drift in the $+M$ direction (Figures 2f and 3f, black curves). The above different motion between the electrons and ions supports the current density that is mostly carried by the electrons in the quiet current sheet (e.g., Lu et al., 2016, 2018a; 2019a). The plasma density peaks at the center of the current sheet (Figure 3d, black curve). At the center of the current sheet, the ion temperature does not increase (Figure 3j, black curve), but the electron temperature slightly increases (Figure 3k, black curve). The energy conversion $\mathbf{j} \cdot \mathbf{E}'$ is about zero in the quiet current sheet (Figures 2 and 3l, black curves).

As the current sheet further thins and the normal magnetic field B_N further decreases, magnetic reconnection begins to occur. In the preliminary reconnection at $\Omega_i t = 68$, B_N breaks through zero from positive to negative at the center of the current sheet (Figure 2a, red curve). The Hall electric field persists and some fine structure of E_L emerges (Figures 2 and 3b, red curves). Because reconnection is preliminary at this time, there is a weak reconnection electric field formed on top of the background convection electric field (Figures 2c and 3c, red curves). The ion flow pattern is identical to that in quiet current sheet (compare black and red curves in Figures 2e, 2f and 3e,

and 3f), whereas the electron flow pattern changes after reconnection occurs (compare black and red curves in Figures 2g, 2h and 3g, and 3h), especially that the electron outflow V_{eL} at $\Omega_i t = 68$ becomes bi-directional on top of that in quiet current sheet (Figure 2g). Moreover, compared to quiet current sheet, the ion temperature does not change (compare black and red curves in Figures 2j and 3j), but the electron temperature changes (compare black and red curves in Figures 2k and 3k). Because of reconnection, the energy conversion from the magnetic field to the plasmas becomes nonzero ($\mathbf{j} \cdot \mathbf{E}' \approx 0.02$) at the reconnection site (Figures 2 and 3l, red curves). Because only electrons respond to the early phase of reconnection, whereas the ions do not, this early phase of reconnection is referred to as electron-only reconnection.

Reconnection then grows fast and becomes well-developed. In the well-developed reconnection at $\Omega_i t = 100$, the Hall electric field E_L and E_N becomes stronger than that in quiet current sheet and electron-only reconnection (Figures 2 and 3b, blue curves) because charge separation, that is, the Hall effect, is enhanced. From electron-only reconnection to this well-developed reconnection, the reconnection electric field E_M is spread and enhanced to ~ 0.1 (Figures 2c and 3c, blue curves). The ion dynamics begins to emerge and couple with reconnection, as shown by the enhanced ion flows (Figures 2e, 2f and 3e, and 3f, blue curves). The ion coupling is also manifested in the ion heating at the center of the reconnection site and even more pronounced in the flow exhausts (Figures 2j and 3j, blue curves). There is a decrease in the ion temperature at the plasma sheet boundary layer $|M| > 2.5d_i$ (Figure 3j, blue curve) caused by betatron cooling due to the decrease in magnetic field from the two previous

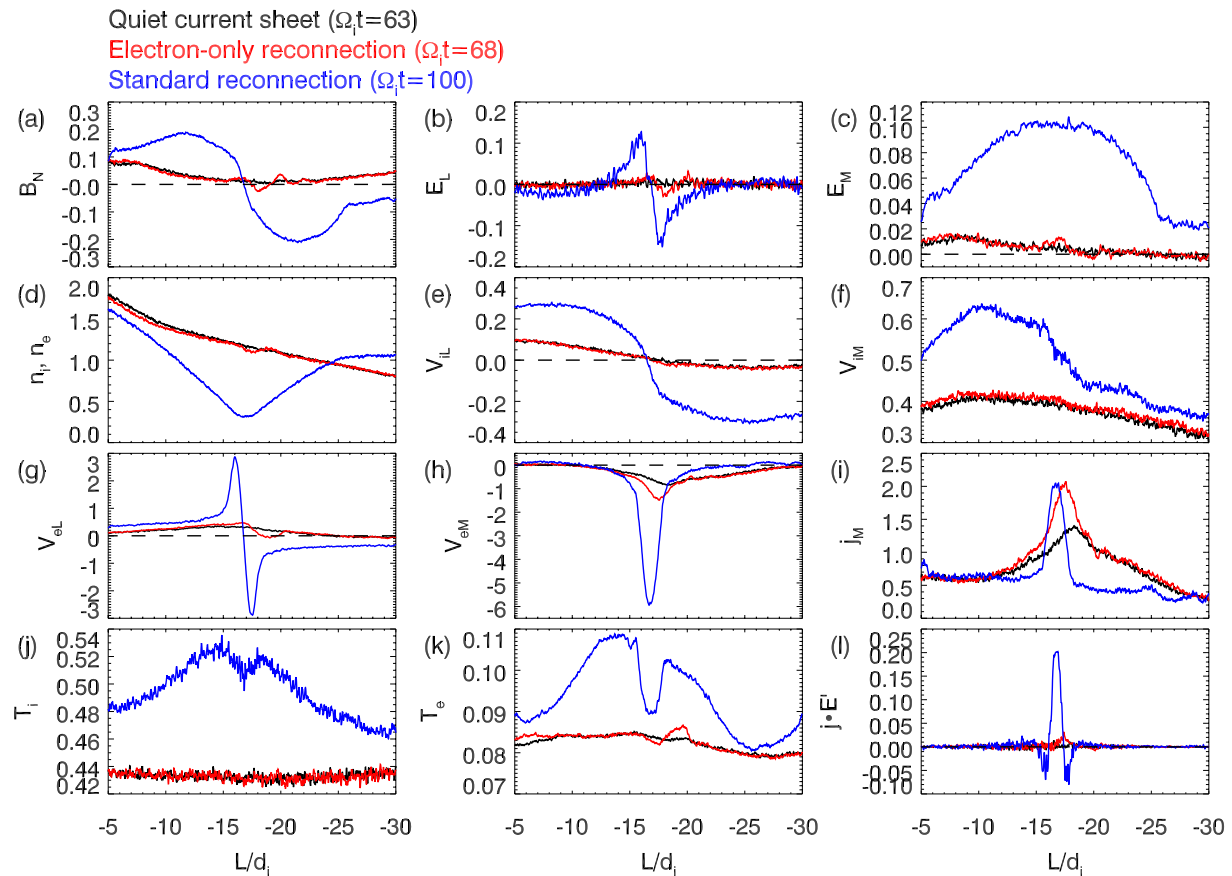


Figure 2. L -profiles, at $N = 0$, of (a) B_N , (b) E_L , (c) E_M , (d) n_i, n_e , (e) V_{iL} , (f) V_{iM} , (g) V_{eL} , (h) V_{eM} , (i) j_M , (j) T_i , (k) T_e , and $\mathbf{j} \cdot \mathbf{E}'$ in quiet current sheet at $\Omega_i t = 63$ (black curves), electron-only reconnection at $\Omega_i t = 68$ (red curves), and standard reconnection at $\Omega_i t = 100$ (blue curves). In our simulation, the magnetic field is in unit of B_0 , the electric field is in unit of $V_A B_0$, plasma density is in unit of n_0 , the velocity is in unit of V_A , the temperature is in unit of $m_i V_A^2$, and $\mathbf{j} \cdot \mathbf{E}'$ is in unit of $en_0 V_A^2 B_0$.

phases to standard reconnection (Figure 3a). For the electron dynamics, the electron flows are further enhanced, and the outflow V_{eL} becomes super-Alfvénic (Figures 2g, 2h and 3g, and 3h, blue curves), and the electrons are heated at the center of the reconnection site and more pronounced in the flow exhausts (Figures 2k and 3k, blue curves). The plasma density is evacuated at the center of the reconnection site (Figure 2d, blue curve). The energy conversion $\mathbf{j} \cdot \mathbf{E}'$ is enhanced to ~ 0.2 (Figures 2 and 3l, blue curves) at the center of the reconnection site. This well-developed reconnection is the standard reconnection that has been well-documented in literature.

4. MMS 17 June 2017 Event

The MMS spacecraft cross an electron-only reconnection event in the normal direction on 17 June 2017 in Earth's magnetotail (Hubbert et al., 2021, 2022; Lu et al., 2020; Wang et al., 2020). In this event, the MMS spacecraft observe fast electron flows in the L and M directions, whereas the ion flows do not increase. However, Farrugia et al. (2021) argue that this event is a standard reconnection event, and the reason why the spacecraft do not observe any ion flow increase in this event is that the spacecraft traverse close to the reconnection site where the ion outflow reverses. Farrugia et al. (2021) also obtain a fast reconnection rate of ~ 0.077 for the MMS 17 June 2017 event based on the reconnection electric field E_M , which is close to the reconnection rate of standard reconnection. However, the reconnection electric field E_M is usually tens of times smaller than the normal electric field E_N (e.g., Torbert et al., 2018), therefore, even a small inaccuracy in the choice of the (L, M, N) coordinate system yields a large error of E_M .

Because of the ambiguity and inaccuracy of the above quantities, we need better criteria to differentiate electron-only reconnection from quiet current sheet and standard reconnection in the magnetotail. Our simulation

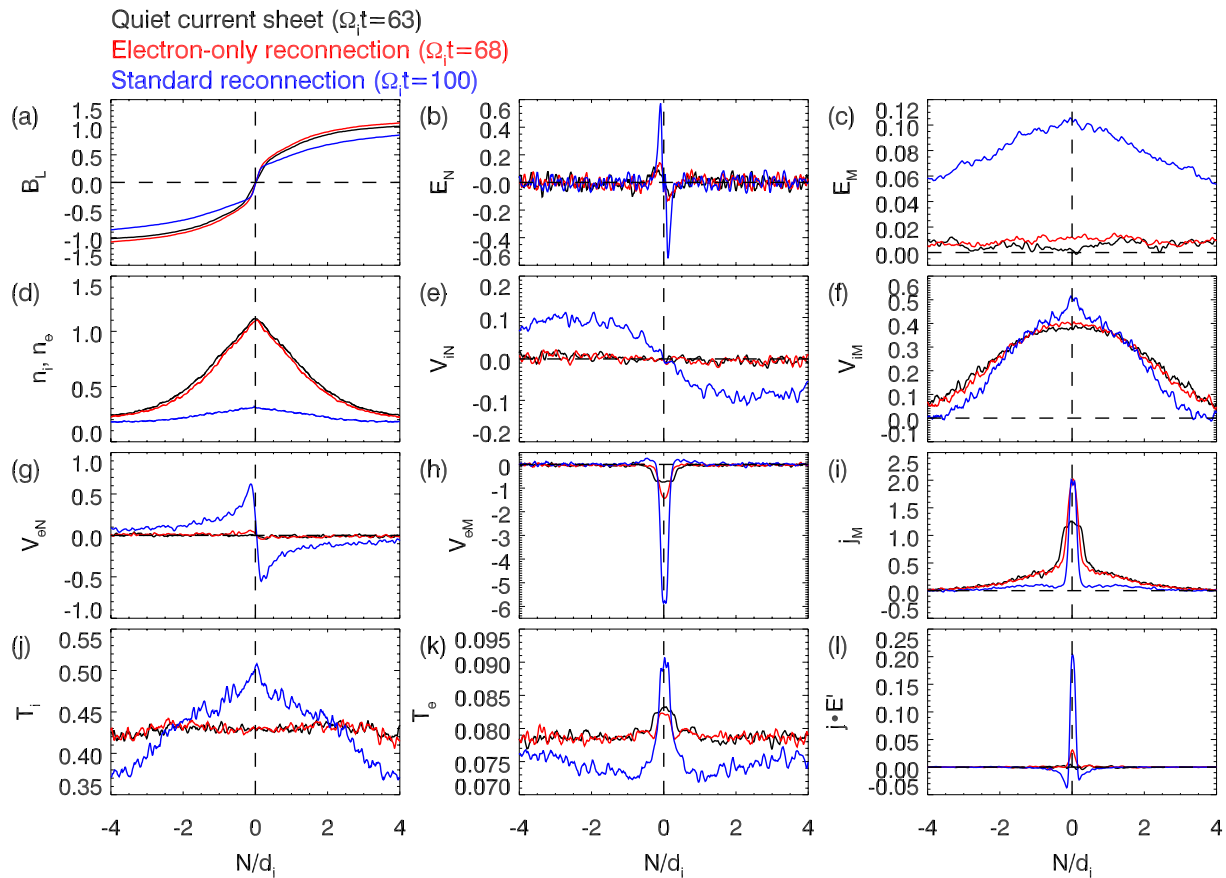


Figure 3. N -profiles of (a) B_L , (b) E_N , (c) E_M , (d) n_i , n_e , (e) V_{iN} , (f) V_{iM} , (g) V_{eN} , (h) V_{eM} , (i) j_M , (j) T_i , (k) T_e , and $\mathbf{j} \cdot \mathbf{E}'$ in quiet current sheet at $\Omega_i t = 63$ (black curves), electron-only reconnection at $\Omega_i t = 68$ (red curves), and standard reconnection at $\Omega_i t = 100$ (blue curves). The profiles at $\Omega_i t = 63$ are along $L/d_i = -19.2$, where B_N at $N = 0$ minimizes, and the profiles at $\Omega_i t = 68$ and $\Omega_i t = 100$ are along $L/d_i = -17.4$ and $L/d_i = -16.8$, respectively, where B_N at $N = 0$ breaks through zero from positive to negative.

results show that the energy conversion $\mathbf{j} \cdot \mathbf{E}'$ is around zero in quiet current sheet but nonzero in electron-only reconnection, which can be used to differentiate electron-only reconnection from quiet current sheet. Moreover, the ion temperature T_i peaks in standard reconnection but does not increase in electron-only reconnection, therefore, it can be used to differentiate electron-only reconnection from standard reconnection. In addition to the above information from snapshots, we further show time histories of reconnection outflows and the two criteria, $\mathbf{j} \cdot \mathbf{E}'$ and T_i , in Figure 4. The occurrence of electron-only reconnection starts from $\Omega_i t \approx 67$ with an abrupt increase in the electron outflow V_{eL} (Figure 4a) and an emergence of nonzero $\mathbf{j} \cdot \mathbf{E}'$ (Figure 4b). Electron-only reconnection then evolves into standard reconnection at $\Omega_i t \approx 78$, after which the ion outflow V_{iL} and the ion temperature T_i increases rapidly (Figures 4c and 4d).

To compare with spacecraft observations, in Figure 5, we plot $\mathbf{j} \cdot \mathbf{E}'$ and T_i versus B_L (a proxy of distance to the center of current sheet, $B_L = 0$). The energy conversion $\mathbf{j} \cdot \mathbf{E}'$ is around zero in quiet current sheet but nonzero in electron-only reconnection and standard reconnection (Figures 5a, 5c and 5e), and the ion temperature does not change across quiet current sheet and electron-only reconnection but peaks at the center of standard reconnection (Figures 5b, 5d and 5f). Note that the ion heating is an intrinsic characteristic of standard reconnection, no matter externally-driven reconnection in the magnetotail current sheet (e.g., Lu et al., 2018b) or spontaneous reconnection in the Harris current sheet (Drake et al., 2009a, 2009b; Lu et al., 2019b). Therefore, Farrugia et al. (2021), using an initial configuration of the Harris current sheet, should have also seen the ion heating in their simulations (although they do not show). Following the above rationale, we plot $\mathbf{j} \cdot \mathbf{E}'$ and T_i in the MMS 17 June 2017 event in Figures 5g and 5h, respectively. The data is from the MMS spacecraft mission (Burch et al., 2016; Ergun et al., 2016; Lindqvist et al., 2016; Pollock et al., 2016; Russell et al., 2016). One can see that in this event, $\mathbf{j} \cdot \mathbf{E}'$ is nonzero at the center, and T_i does not increase, so this event is a magnetotail electron-only reconnection event.

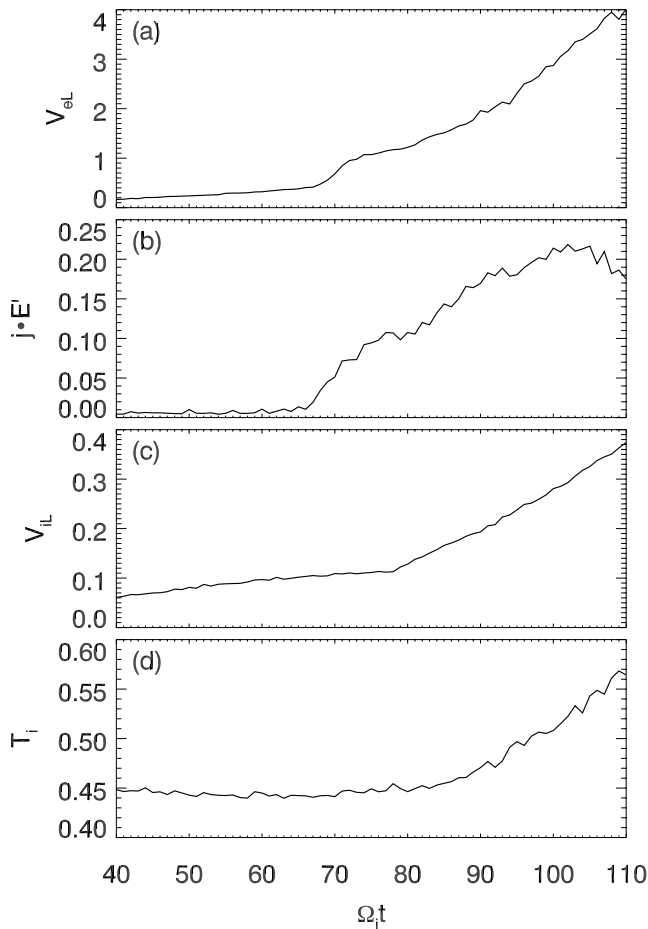


Figure 4. Time histories of (a and c) the maximum electron and ion outflows in the L direction V_{eL} and V_{iL} at $N = 0$ and (b and d) the maximum energy conversion $\mathbf{j} \cdot \mathbf{E}'$ and ion temperature T_i at $L = L_R$. Here L_R is where B_N at $N = 0$ minimizes before reconnection and reverses after reconnection.

5. Conclusions and Discussion

The main conclusions are summarized as follows:

1. In the magnetotail, because of a strong external driver, quiet current sheet with a sub ion scale thickness and a small B_N is formed, and then electron-only reconnection emerges in this current sheet. In electron-only reconnection, electron flows and electron temperature increase, whereas ion flows and ion temperature do not change. The energy conversion $\mathbf{j} \cdot \mathbf{E}'$ becomes nonzero and peaks around the electron-only reconnection site, whereas $\mathbf{j} \cdot \mathbf{E}'$ is about zero in quiet current sheet. This criterion of $\mathbf{j} \cdot \mathbf{E}'$ can be used to differentiate electron-only reconnection from quiet current sheet.
2. Electron-only reconnection then proceeds to standard reconnection with significant enhancements in the reconnected magnetic field, the Hall electric field, the reconnection electric field, the energy conversion $\mathbf{j} \cdot \mathbf{E}'$, electron flows, and electron temperature. In standard reconnection, ion dynamics emerges with an increase in ion flows and ion temperature. The increase in ion temperature can be used as a criterion to differentiate electron-only reconnection from standard reconnection in the magnetotail.
3. In the MMS 17 June 2017 event, $\mathbf{j} \cdot \mathbf{E}'$ is nonzero and ion temperature does not increase. Based on the above two criteria, we justify that this event is an electron-only reconnection event in the magnetotail.

We show that electron-only reconnection can be the early phase of magnetotail reconnection when reconnection is preliminary and overlooked by the ions. Such magnetotail electron-only reconnection is different from that in turbulent plasma environments, for example, the magnetosheath, in which reconnection is electron-only because it is confined to a small region so that ions do not respond to it (e.g., Phan et al., 2018; Pyakurel et al., 2019, 2021; Stawarz et al., 2022). In magnetotail electron-only reconnection, the sub ion scale electron current sheet is embedded in a thicker ion scale current sheet (Figure 3i), which is different from that in turbulence electron-only reconnection. Moreover, turbulence electron-only reconnection usually produces super-Alfvénic electron outflows, but the electron outflow in magnetotail electron-only reconnection is much slower (not necessarily super-Alfvénic) because the electrons are not sufficiently accelerated in the preliminary reconnection. Also note that in magnetotail electron-only reconnection, there is some nonzero but weak ion flow, $V_{iL} \approx 0.1V_A$, corresponding to about tens of km/s in the magnetotail. This weak ion flow is caused not by reconnection but by the background plasma environment, such as the external driver or convection in the neighborhood.

electron-only reconnection is much slower (not necessarily super-Alfvénic) because the electrons are not sufficiently accelerated in the preliminary reconnection. Also note that in magnetotail electron-only reconnection, there is some nonzero but weak ion flow, $V_{iL} \approx 0.1V_A$, corresponding to about tens of km/s in the magnetotail. This weak ion flow is caused not by reconnection but by the background plasma environment, such as the external driver or convection in the neighborhood.

The time- and spatial scales of magnetotail electron-only reconnection determine how likely it is to be observed by MMS. As shown in Figure 4, the duration of magnetotail electron-only reconnection is about $10\Omega_i^{-1}$, corresponding to ~ 5 – 10 s for the typical magnetotail parameters, and its spatial scale is sub ion scale (~ 100 km). The high-resolution MMS measurements are capable to resolve this. Note that the 5–10 s duration is long enough for MMS to cross through the electron-only reconnection (the 17 June 2017 crossing duration is ~ 2 s) before it evolves into standard reconnection. Moreover, theoretical analyses and simulations have shown that the electron tearing mode responsible for magnetotail electron-only reconnection has a large wavenumber in the L direction, $k_L d_i \sim 1$ (e.g., Brittnacher et al., 1995; Lu et al., 2019b; Pritchett et al., 1991). Therefore, it should not be difficult for MMS to detect magnetotail electron-only reconnection. And indeed, Hubbert et al. (2021, 2022) have reported more than ten electron-only reconnection events in the magnetotail.

The nonzero energy conversion $\mathbf{j} \cdot \mathbf{E}$ or $\mathbf{j} \cdot \mathbf{E}'$ exists not only in reconnection but also in other magnetotail processes and structures, such as dipolarization fronts (e.g., Khotyaintsev et al., 2017; Shu et al., 2021). The present study focuses on reconnection, but for more general circumstances of nonzero energy conversion, one

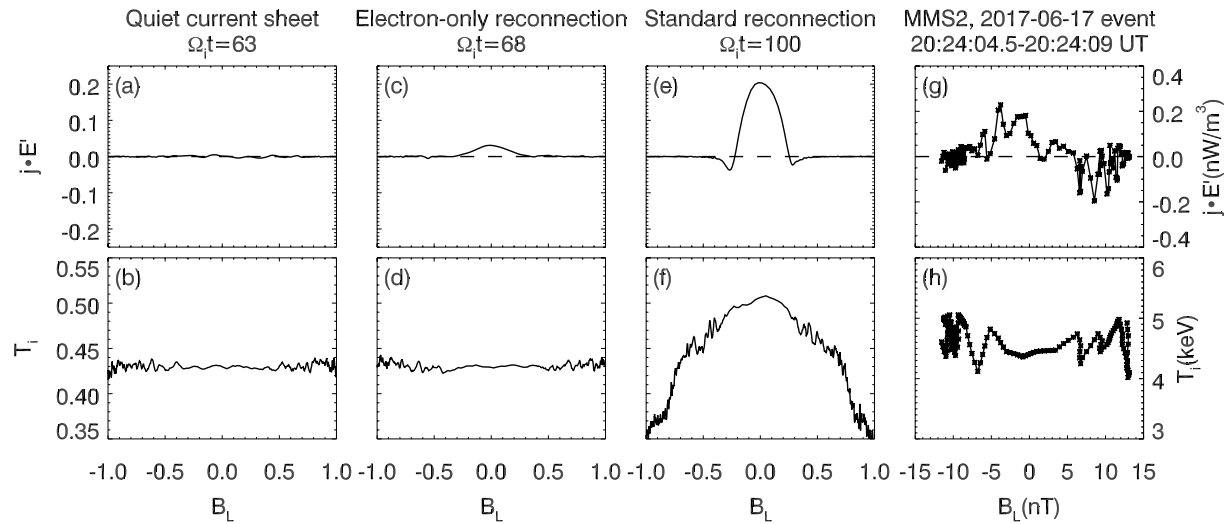


Figure 5. Energy conversion $\mathbf{j} \cdot \mathbf{E}'$ (top panels) and ion temperature T_i (bottom panels) as function of B_L from our simulation in (a and b) quiet current sheet at $\Omega_i t = 63$, (c and d) electron-only reconnection at $\Omega_i t = 68$, and (e and f) standard reconnection at $\Omega_i t = 100$. The profiles at $\Omega_i t = 63$ are along $L/d_i = -19.2$, where B_N at $N = 0$ minimizes, and the profiles at $\Omega_i t = 68$ and $\Omega_i t = 100$ are along $L/d_i = -17.4$ and $L/d_i = -16.8$, respectively, where B_N at $N = 0$ breaks through zero from positive to negative. Here B_L is a proxy of distance to the center of current sheet ($B_L = 0$). (g and h) Energy conversion $\mathbf{j} \cdot \mathbf{E}'$ and ion temperature T_i as function of B_L observed by MMS2 from 20:24:04.5 to 20:24:09 UT on 17 June 2017. The MMS data is also shown in the local (L, M, N) coordinate system, with $L = (0.9477, 0.3023, -0.1029)$, $M = (-0.0855, -0.0703, -0.9939)$, and $N = (-0.3076, 0.9506, -0.0408)$ in the geocentric solar ecliptic (GSE) coordinate system. The current density is calculated using $\mathbf{j} = en_e(\mathbf{V}_i - \mathbf{V}_e)$. Because the measurements of electron moments, ion moments, electric field, and magnetic field have different resolutions, we interpolate the ion moments, electric field and magnetic field measurements to that of the electron moments to compute $\mathbf{j} \cdot \mathbf{E}'$.

needs to consider other specific characteristics (e.g., sharp increase in B_z for dipolarization fronts) for differentiation. Note that the demonstration in the present study is mostly qualitative, and to have a more quantitative sense, for typical magnetotail values of $B_0 = 20$ nT and $n_0 = 0.3$ cm $^{-3}$, the corresponding $\mathbf{j} \cdot \mathbf{E}'$ is about $0.03en_0V_A^2B_0 \sim 0.02$ nW/m 3 in electron-only reconnection and about $0.2en_0V_A^2B_0 \sim 0.12$ nW/m 3 in standard reconnection, and the ion temperature T_i is about $0.43m_iV_A^2 \sim 2.9$ keV in pre-reconnection current sheet and electron-only reconnection and about $0.51m_iV_A^2 \sim 3.4$ keV in standard reconnection. However, it is important to note that the above T_i depends on its initial value, distribution, and background value, and the exact value of $\mathbf{j} \cdot \mathbf{E}'$ obtained from PIC simulations can be underestimated because the mass ratio and speed of light in PIC simulations are smaller than realistic. Moreover, in spacecraft observations, the values of T_i , $\mathbf{j} \cdot \mathbf{E}'$, etc. also vary in different events because the environmental plasma parameters and spacecraft trajectories are different. For the above reasons, here we preferentially focus on the qualitative and distinct differences because they are simulation setup agnostic and applicable for more observational events.

Data Availability Statement

The simulation data is archived in <https://doi.org/10.6084/m9.figshare.19262366.v2>. The MMS spacecraft data are publicly available at the MMS science data center (<https://lasp.colorado.edu/mms/sdc/public/about/browse-wrapper/>).

Acknowledgments

This work was supported by Key Research Program of Frontier Sciences CAS (QYZDJ-SSW-DQC010) and NSFC 42174181.

References

- Birn, J., Drake, J. F., Shay, M. A., Rogers, B. N., Denton, R. E., Hesse, M., et al. (2001). Geospace environmental modeling (GEM) magnetic reconnection challenge. *Journal of Geophysical Research*, *106*(A3), 3715–3719. <https://doi.org/10.1029/1999ja900449>
- Birn, J., & Hesse, M. (2014). Forced reconnection in the near magnetotail: Onset and energy conversion in PIC and MHD simulations. *Journal of Geophysical Research: Space Physics*, *119*, 290–309. <https://doi.org/10.1002/2013ja019354>
- Birn, J., & Priest, E. R. (2007). *Reconnection of magnetic fields: Magnetohydrodynamics and collisionless theory and observations*. Cambridge University Press.
- Borg, A. L., Oieroset, M., Phan, T. D., Mozer, F. S., Pedersen, A., Mouikis, C., et al. (2005). Cluster encounter of a magnetic reconnection diffusion region in the near-Earth magnetotail on September 19, 2003. *Geophysical Research Letters*, *32*(19), L19105. <https://doi.org/10.1029/2005gl023794>
- Brittnacher, M., Quest, K. B., & Karimabadi, H. (1995). A new approach to the linear-theory of single-species tearing in 2-dimensional quasi-neutral sheets. *Journal of Geophysical Research*, *100*(A3), 3551–3562. <https://doi.org/10.1029/94ja02743>

- Burch, J. L., Moore, T. E., Torbert, R. B., & Giles, B. L. (2016). Magnetospheric multiscale overview and science objectives. *Space Science Reviews*, 199(1–4), 5–21. <https://doi.org/10.1007/s11214-015-0164-9>
- Drake, J. F., Cassak, P. A., Shay, M. A., Swisdak, M., & Quataert, E. (2009). A magnetic reconnection mechanism for ion acceleration and abundance enhancements in impulsive flares. *The Astrophysical Journal Letters*, 700(1), L16–L20. <https://doi.org/10.1088/0004-637x/700/1/L16>
- Drake, J. F., Swisdak, M., Phan, T. D., Cassak, P. A., Shay, M. A., Lepri, S. T., et al. (2009). Ion heating resulting from pickup in magnetic reconnection exhausts. *Journal of Geophysical Research*, 114(A5), A05111. <https://doi.org/10.1029/2008ja013701>
- Eastwood, J. P., Phan, T. D., Oieroset, M., & Shay, M. A. (2010). Average properties of the magnetic reconnection ion diffusion region in the Earth's magnetotail: The 2001–2005 Cluster observations and comparison with simulations. *Journal of Geophysical Research*, 115(A8), A08215. <https://doi.org/10.1029/2009ja014962>
- Ergun, R. E., Tucker, S., Westfall, J., Goodrich, K. A., Malaspina, D. M., Summers, D., et al. (2016). The axial double probe and fields signal processing for the MMS mission. *Space Science Reviews*, 199(1–4), 167–188. <https://doi.org/10.1007/s11214-014-0115-x>
- Farrugia, C. J., Rogers, A. J., Torbert, R. B., Genestreti, K. J., Nakamura, T. K. M., Lavraud, B., et al. (2021). An encounter with the ion and electron diffusion regions at a flapping and twisted tail current sheet. *Journal of Geophysical Research: Space Physics*, 126, e2020JA028903. <https://doi.org/10.1029/2020JA028903>
- Fu, X. R., Lu, Q. M., & Wang, S. (2006). The process of electron acceleration during collisionless magnetic reconnection. *Physics of Plasmas*, 13(1), 012309. <https://doi.org/10.1063/1.2164808>
- Galeev, A. A., & Zelenyi, L. M. (1976). Tearing instability in plasma configurations. *Zhurnal Eksperimentalnoi I Teoreticheskoi Fiziki*, 70, 2133–2151.
- Gingell, I., Schwartz, S. J., Eastwood, J. P., Burch, J. L., Ergun, R. E., Fuselier, S., et al. (2019). Observations of magnetic reconnection in the transition region of quasi-parallel shocks. *Geophysical Research Letters*, 46(3), 1177–1184. <https://doi.org/10.1029/2018gl081804>
- Gingell, I., Schwartz, S. J., Eastwood, J. P., Stawarz, J. E., Burch, J. L., Ergun, R. E., et al. (2020). Statistics of reconnecting current sheets in the transition region of earth's bow shock. *Journal of Geophysical Research: Space Physics*, 125, e2019JA027119. <https://doi.org/10.1029/2019JA027119>
- Hesse, M., Aunai, N., Sibeck, D., & Birn, J. (2014). On the electron diffusion region in planar, asymmetric, systems. *Geophysical Research Letters*, 41(24), 8673–8680. <https://doi.org/10.1002/2014gl061586>
- Hesse, M., Birn, J., & Kuznetsova, M. (2001). Collisionless magnetic reconnection: Electron processes and transport modeling. *Journal of Geophysical Research*, 106(A3), 3721–3735. <https://doi.org/10.1029/1999ja001002>
- Hesse, M., & Schindler, K. (2001). The onset of magnetic reconnection in the magnetotail. *Earth Planets and Space*, 53(6), 645–653. <https://doi.org/10.1186/Bf03353284>
- Hoshino, M., Mukai, T., Terasawa, T., & Shinohara, I. (2001). Suprathermal electron acceleration in magnetic reconnection. *Journal of Geophysical Research*, 106(A11), 25979–25997. <https://doi.org/10.1029/2001ja900052>
- Huang, C., Lu, Q. M., & Wang, S. (2010). The mechanisms of electron acceleration in antiparallel and guide field magnetic reconnection. *Physics of Plasmas*, 17(7), 072306. <https://doi.org/10.1063/1.3457930>
- Hubbert, M., Qi, Y., Russell, C. T., Burch, J. L., Giles, B. L., & Moore, T. E. (2021). Electron-Only tail current sheets and their temporal evolution. *Geophysical Research Letters*, 48(5), e2020GL091364. <https://doi.org/10.1029/2020GL091364>
- Hubbert, M., Russell, C. T., Qi, Y., Lu, S., Burch, J. L., Giles, B. L., & Moore, T. E. (2022). Electron-only reconnection as a transition phase from quiet current sheet to traditional magnetotail reconnection. *Journal of Geophysical Research: Space Physics*, 127, e2021JA029584. <https://doi.org/10.1029/2021JA029584>
- Khotyaintsev, Y. V., Divin, A., Vaivads, A., Andre, M., & Markidis, S. (2017). Energy conversion at dipolarization fronts. *Geophysical Research Letters*, 44(3), 1234–1242. <https://doi.org/10.1002/2016GL071909>
- Lembege, B., & Pellat, R. (1982). Stability of a thick two-dimensional quasi-neutral sheet. *Physics of Fluids*, 25(11), 1995–2004. <https://doi.org/10.1063/1.863677>
- Lindqvist, P. A., Olsson, G., Torbert, R. B., King, B., Granoff, M., Rau, D., et al. (2016). The spin-plane double probe electric field instrument for MMS. *Space Science Reviews*, 199(1–4), 137–165. <https://doi.org/10.1007/s11214-014-0116-9>
- Liu, Y.-H., Birn, J., Daughton, W., Hesse, M., & Schindler, K. (2014). Onset of reconnection in the near magnetotail: PIC simulations. *Journal of Geophysical Research: Space Physics*, 119(12), 9773–9789. <https://doi.org/10.1002/2014ja020492>
- Lu, Q. M., Huang, C., Xie, J. L., Wang, R. S., Wu, M. Y., Vaivads, A., & Wang, S. (2010). Features of separatrix regions in magnetic reconnection: Comparison of 2-D particle-in-cell simulations and Cluster observations. *Journal of Geophysical Research*, 115, A11208. <https://doi.org/10.1029/2010ja015713>
- Lu, Q. M., Yang, Z. W., Wang, H. Y., Wang, R. S., Huang, K., Lu, S., & Wang, S. (2021). Two-dimensional particle-in-cell simulation of magnetic reconnection in the downstream of a quasi-perpendicular shock. *The Astrophysical Journal*, 919(1), 28. <https://doi.org/10.3847/1538-4357/919/1/28>
- Lu, S., Angelopoulos, V., Artemyev, A. V., Pritchett, P. L., Liu, J., Runov, A., et al. (2019). Turbulence and particle acceleration in collisionless magnetic reconnection: Effects of temperature inhomogeneity across pre-reconnection current sheet. *The Astrophysical Journal*, 878(2), 109. <https://doi.org/10.3847/1538-4357/ab1f6b>
- Lu, S., Artemyev, A. V., Angelopoulos, V., Lin, Y., Zhang, X.-J., Liu, J., & Strangeway, R. J. (2019). The Hall electric field in Earth's magnetotail thin current sheet. *Journal of Geophysical Research: Space Physics*, 124, 1052–1062. <https://doi.org/10.1029/2018JA026202>
- Lu, S., Lin, Y., Angelopoulos, V., Artemyev, A. V., Pritchett, P. L., Lu, Q. M., & Wang, X. Y. (2016). Hall effect control of magnetotail dawn-dusk asymmetry: A three-dimensional global hybrid simulation. *Journal of Geophysical Research: Space Physics*, 121, 11882–11895. <https://doi.org/10.1002/2016JA023325>
- Lu, S., Pritchett, P. L., Angelopoulos, V., & Artemyev, A. V. (2018a). Formation of dawn-dusk asymmetry in earth's magnetotail thin current sheet: A three-dimensional particle-in-cell simulation. *Journal of Geophysical Research: Space Physics*, 123, 2801–2814. <https://doi.org/10.1002/2017JA025095>
- Lu, S., Pritchett, P. L., Angelopoulos, V., & Artemyev, A. V. (2018b). Magnetic reconnection in Earth's magnetotail: Energy conversion and its earthward-tailward asymmetry. *Physics of Plasmas*, 25(1), 012905. <https://doi.org/10.1063/1.5016435>
- Lu, S., Wang, R. S., Lu, Q. M., Angelopoulos, V., Nakamura, R., Artemyev, A. V., et al. (2020). Magnetotail reconnection onset caused by electron kinetics with a strong external driver. *Nature Communications*, 11(1), 5049. <https://doi.org/10.1038/s41467-020-18787-w>
- Ma, Z. W., & Bhattacharjee, A. (2001). Hall magnetohydrodynamic reconnection: The Geospace Environment Modeling challenge. *Journal of Geophysical Research*, 106(A3), 3773–3782. <https://doi.org/10.1029/1999ja001004>
- Nagai, T., Shinohara, I., Fujimoto, M., Hoshino, M., Saito, Y., Machida, S., & Mukai, T. (2001). Geotail observations of the Hall current system: Evidence of magnetic reconnection in the magnetotail. *Journal of Geophysical Research*, 106(A11), 25929–25949. <https://doi.org/10.1029/2001ja900038>

- Øieroset, M., Phan, T. D., Fujimoto, M., Lin, R. P., & Lepping, R. P. (2001). In situ detection of collisionless reconnection in the Earth's magnetotail. *Nature*, *412*(6845), 414–417. <https://doi.org/10.1038/35086520>
- Pellat, R., Coroniti, F. V., & Pritchett, P. L. (1991). Does ion tearing exist. *Geophysical Research Letters*, *18*(2), 143–146. <https://doi.org/10.1029/91gl00123>
- Phan, T. D., Eastwood, J. P., Shay, M. A., Drake, J. F., Sonnerup, B. U. O., Fujimoto, M., et al. (2018). Electron magnetic reconnection without ion coupling in Earth's turbulent magnetosheath. *Nature*, *557*(7704), 202–206. <https://doi.org/10.1038/s41586-018-0091-5>
- Pollock, C., Moore, T., Jacques, A., Burch, J., Gliese, U., Saito, Y., et al. (2016). Fast plasma investigation for magnetospheric multiscale. *Space Science Reviews*, *199*(1–4), 331–406. <https://doi.org/10.1007/s11214-016-0245-4>
- Pritchett, P. L. (2001). Geospace Environment Modeling magnetic reconnection challenge: Simulations with a full particle electromagnetic code. *Journal of Geophysical Research*, *106*(A3), 3783–3798. <https://doi.org/10.1029/1999ja001006>
- Pritchett, P. L. (2005a). Externally driven magnetic reconnection in the presence of a normal magnetic field. *Journal of Geophysical Research*, *110*(A5), A05209. <https://doi.org/10.1029/2004ja010948>
- Pritchett, P. L. (2005b). The "Newton Challenge": Kinetic aspects of forced magnetic reconnection. *Journal of Geophysical Research*, *110*(A10), A10213. <https://doi.org/10.1029/2005ja011228>
- Pritchett, P. L. (2010). Onset of magnetic reconnection in the presence of a normal magnetic field: Realistic ion to electron mass ratio. *Journal of Geophysical Research*, *115*(A10), A10208. <https://doi.org/10.1029/2010ja015371>
- Pritchett, P. L., Coroniti, F. V., Pellat, R., & Karimabadi, H. (1991). Collisionless reconnection in 2-dimensional magnetotail equilibria. *Journal of Geophysical Research*, *96*(A7), 11523–11538. <https://doi.org/10.1029/91ja01094>
- Pritchett, P. L., & Lu, S. (2018). Externally driven onset of localized magnetic reconnection and disruption in a magnetotail configuration. *Journal of Geophysical Research: Space Physics*, *123*, 2787–2800. <https://doi.org/10.1002/2017ja025094>
- Pyakurel, P. S., Shay, M. A., Drake, J. F., Phan, T. D., Cassak, P. A., & Verniero, J. L. (2021). Faster form of electron magnetic reconnection with a finite length X-line. *Physical Review Letters*, *127*(15), 155101. <https://doi.org/10.1103/PhysRevLett.127.155101>
- Pyakurel, P. S., Shay, M. A., Phan, T. D., Matthaeus, W. H., Drake, J. F., TenBarge, J. M., et al. (2019). Transition from ion-coupled to electron-only reconnection: Basic physics and implications for plasma turbulence. *Physics of Plasmas*, *26*(8), 082307. <https://doi.org/10.1063/1.5090403>
- Retinò, A., Sundkvist, D., Vaivads, A., Mozer, F., André, M., & Owen, C. J. (2007). In situ evidence of magnetic reconnection in turbulent plasma. *Nature Physics*, *3*(4), 235–238. <https://doi.org/10.1038/nphys574>
- Russell, C. T., Anderson, B. J., Baumjohann, W., Bromund, K. R., Dearborn, D., Fischer, D., et al. (2016). The magnetospheric multiscale magnetometers. *Space Science Reviews*, *199*(1–4), 189–256. <https://doi.org/10.1007/s11214-014-0057-3>
- Shay, M. A., Drake, J. F., Rogers, B. N., & Denton, R. E. (2001). Alfvénic collisionless magnetic reconnection and the Hall term. *Journal of Geophysical Research*, *106*(A3), 3759–3772. <https://doi.org/10.1029/1999ja001007>
- Shay, M. A., Drake, J. F., & Swisdak, M. (2007). Two-scale structure of the electron dissipation region during collisionless magnetic reconnection. *Physical Review Letters*, *99*(15), 155002. <https://doi.org/10.1103/PhysRevLett.99.155002>
- Shu, Y. K., Lu, S., Lu, Q. M., Ding, W. X., & Wang, S. (2021). Energy budgets from collisionless magnetic reconnection site to reconnection front. *Journal of Geophysical Research: Space Physics*, *126*, e2021JA029712. <https://doi.org/10.1029/2021JA029712>
- Stawarz, J. E., Eastwood, J. P., Phan, T. D., Gingell, I. L., Pyakurel, P. S., Shay, M. A., et al. (2022). Turbulence-driven magnetic reconnection and the magnetic correlation length: Observations from Magnetospheric Multiscale in Earth's magnetosheath. *Physics of Plasmas*, *29*(1), 012302. <https://doi.org/10.1063/5.0071106>
- Stawarz, J. E., Eastwood, J. P., Phan, T. D., Gingell, I. L., Shay, M. A., Burch, J. L., et al. (2019). Properties of the turbulence associated with electron-only magnetic reconnection in earth's magnetosheath. *The Astrophysical Journal Letters*, *877*(2), L37. <https://doi.org/10.3847/2041-8213/ab21c8>
- Torbert, R. B., Burch, J. L., Phan, T. D., Hesse, M., Argall, M. R., Shuster, J., et al. (2018). Electron-scale dynamics of the diffusion region during symmetric magnetic reconnection in space. *Science*, *362*(6421), 1391–1395. <https://doi.org/10.1126/science.aat2998>
- Wang, R. S., Lu, Q. M., Lu, S., Russell, C. T., Burch, J. L., Gershman, D. J., et al. (2020). Physical implication of two types of reconnection electron diffusion regions with and without ion-coupling in the magnetotail current sheet. *Geophysical Research Letters*, *47*(21), e2020GL088761. <https://doi.org/10.1029/2020GL088761>
- Yamada, M., Kulsrud, R., & Ji, H. T. (2010). Magnetic reconnection. *Reviews of Modern Physics*, *82*(1), 603–664. <https://doi.org/10.1103/RevModPhys.82.603>
- Zenitani, S., Hesse, M., Klimas, A., & Kuznetsova, M. (2011). New measure of the dissipation region in collisionless magnetic reconnection. *Physical Review Letters*, *106*(19), 195003. <https://doi.org/10.1103/PhysRevLett.106.195003>